

Study on Finite Element Method of Stress Field in Aluminum Alloy High-Speed Milling Process

Wei Zhang^{1*}, Shunming Li², Qijun Wu¹, Zenghui An²

¹China Ship Development and Design Center Wuhan, China

²College of Energy and Power Engineering Nanjing University of Aeronautics and Astronautics Nanjing, China

Abstract. Three-dimensional numerical simulation model has been built by means of Advantage FEM. Perform simulation the stress fields of 7050-T7451 aluminum alloy in high speed milling process at the speed range of 628 m/min~5946 m/min. The dynamic change and speed's influence of stress fields and residual stress in machined layer is systematically analyzed. Some conclusions were drawn. With the cutting process development, the stress field converts to the stress state that crushing stress occupies a leading position. The magnitudes of crushing stress in all directions reduce with milling processes as the effect of Thermal-Mechanical-Coupled weakens; With the cutting speed increasing the magnitudes of crushing stress in all directions fluctuate near -950Mpa first, and then increase at the speed of 3000m/min; The residual pulling stress beneath the surface 0.03mm has been found and the magnitude increases with the cutting speed. A good agreement was obtained between predictions and experiments.

1. Introduction

High speed cutting generally involves a large amount of plastic deformation and is coupled high temperature, high strain rate and large strain processes [1, 2]. It always comes with non-uniform Thermal-Mechanical-Coupled stress field on machined layer [3, 4]. The large plastic deformation process and sever friction condition in the chip-tool-workpiece contact zone has important influence on mechanism of deformation and microstructure, work-hardening and residual stress in machined layer [5, 6].

High speed milling is a process which is typical periodicity interrupted cutting [7]. Machined surface is arisen from the process of plastic deformation as the result of cutting force and the changing temperature process which is heating and cooling. The machined surface of high speed milling process relative to conventional cutting appears the non-uniform serious stress field introduced from the frictional behavior between cutting tool flank and workpiece [8]. The theory that the non-uniform serious stress field form on the machined surface is based on the deformation theory and tribology of high speed milling process [9, 10]. The study of non-uniform Thermal-Mechanical-Coupled stress field on machined layer play an important role in the research on chip formation mechanism, the failure mechanism of cutting tool and improving the surface quality of workpiece [11].



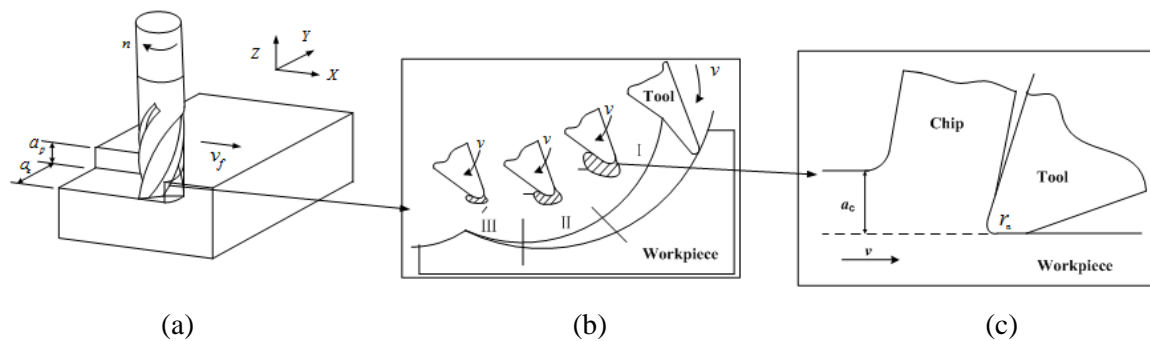


Figure 1. Three-dimensional model of high speed milling process.

As figure 1(b) shows, when viewed from a narrow perspective, single-point tool similar to single edge oblique cutting. There are three phases of deformation in high speed milling process: shear, extrusion and slippage. This cutting process could be reduced to the orthogonal cutting model (figure 1(c)). But the simplified model can cause inaccurate results. Three-dimensional numerical simulation has been introduced in this work. The cutting speed within 628~5946m/min is of main interest. The study can provide data basis for the prediction of the flow stress, the research on the failure mechanism of cutting tool and so on.

2. Finite element aspects and material modeling

2.1. Material modeling

050-T7451 is Al-Zn-Mg-Cu-Zr alloy with high strength, high resistance to stress-corrosion cracking and good fracture toughness. The physical mechanical properties and composition of 7050-T7451 are provided in table 1, 2 [12].

Table 1. Physical mechanical properties of 7050-T7451 aluminum alloy.

Thermal Conductivity W/(m·K)	Heat Capacity J/(kg·K)	Density Kg/m ³	Alpha 10 ⁻⁵ /K	Poisson's Ratio	Young's Modulus 10 ¹⁰ Pa
180	860	2830	2.54	0.33	7.17

Table 2. Chemical composition of 7050-T7451 aluminum alloy.

w(Si)	w(Fe)	w(Cu)	w(Mn)	w(Mg)	w(Cr)	w(Zn)	w(Ti)	w(B)	w(Al)
0.057	0.119	2.2	0.016	2.21	0.012	6.28	0.0332	0.0006	Bal.

For the description of the deformation localization during high speed load the model of Johnson-Cook [13] (equation 1) turned out to be appropriate because of its viscoplastic flowing regulation in the form of an exponential function.

$$\sigma = \left[A + B(\varepsilon)^n \right] \left[1 + C \ln \left(\frac{\dot{\varepsilon}}{\dot{\varepsilon}_0} \right) \right] \left[1 - \left(\frac{T - T_0}{T_m - T_0} \right)^m \right] \quad (1)$$

where coefficient A (MPa) is the yield strength; B (MPa) the hardening modulus; C the strain rate sensitivity coefficient; n the hardening coefficient; m is the thermal softening coefficient. $\dot{\varepsilon}_0$ the reference plastic strain rate (s⁻¹); σ is the flow stress; ε the plastic strain; $\dot{\varepsilon}$ the strain rate (s⁻¹); T (°C) the workpiece temperature; T_m (635°C) the melting temperature of the workpiece material; T_0 (25 °C) is the room temperature. Table 3 reports the material constants obtained by Fu Xiuli's [14] researches.

Table 3. Johnson Cook material parameters.

Variable	$\dot{\varepsilon}_0$ (s ⁻¹)	A(MPa)	B(MPa)	C	n	m
value	1	463.4	319.5	0.027	0.32	0.99

2.1.1. Cutting parameters. The cutting parameters have been selected based on the high speed experiment. Detailed parameters go as follows (table 4)

Table 4. Cutting condition.

Cutting Speed	628~5946 m/min
Other Parameters	$f_z=0.15\text{mm/z}$, $a_p=3\text{mm}$, $a_e=12\text{mm}$
tool	YG6X
	$\gamma_0=25^\circ$, $\alpha_0=6^\circ$, $d=30\text{mm}$, $r_n=0.02\text{mm}$

3. Near-surface stress field of high speed milling process

3.1. Dynamic analysis of stress field

Figure 2 illustrates the stress distribution in all directions when the cutting speed is 5026m/min. As you can see from this figure, the non-uniform serious stress field is found mainly in primary shear zone near the tool tip. The stress field is very complex during the initial phase of the cutting process, which shows the phenomenon of interlacing pulling stress and crushing stress. With the cutting process development, the stress field converts to the stress state that crushing stress occupies a leading position. This stress field introduced from high-speed milling could help to improve the surface quality.

The variation on stress field of machined layer in the whole high speed process is shown in figure 3(a). Obviously, the magnitude of Stress-XX is slightly bigger than Stress-YY. The magnitudes of crushing stress in all directions reduce with milling processes. A trend can be derived from figure 3(b), which is that the temperature and cutting force all reduce with milling processes. This is because the practical cutting thickness attenuates in the whole high speed process as the result of the trochoid theory of down milling. This trend leads to the effect of Thermal-Mechanical-Coupled weaken. The stress field of layer is the net result.

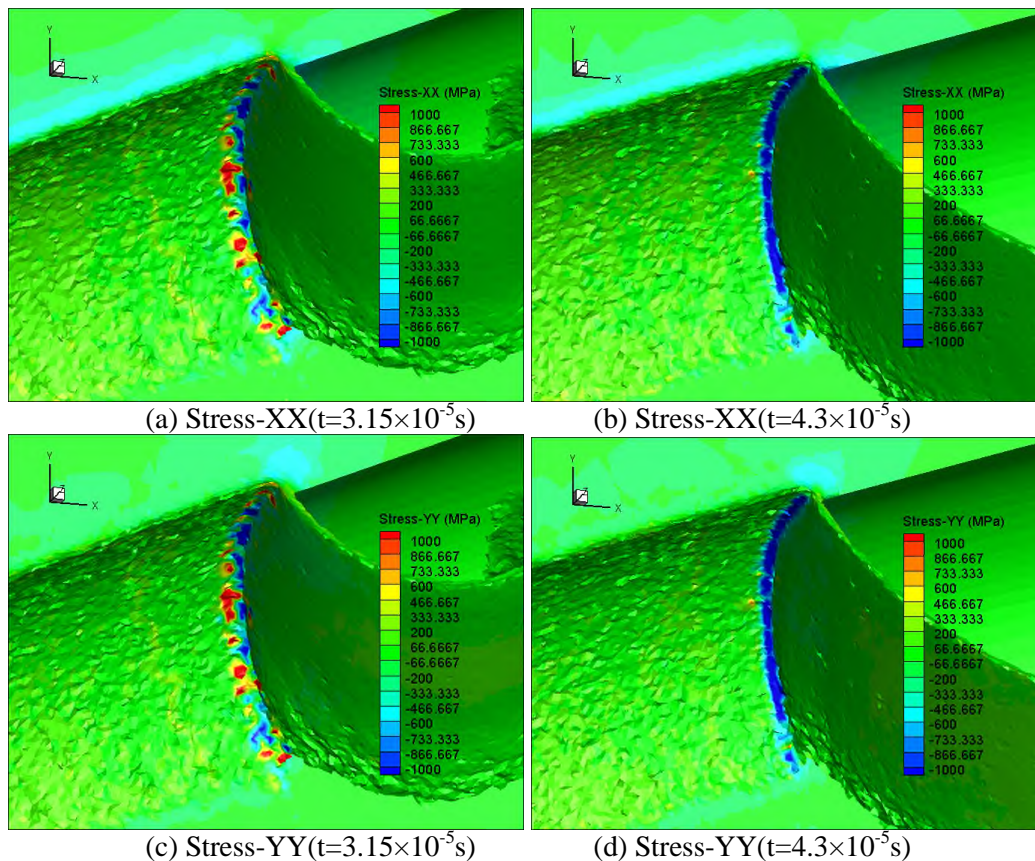


Figure 2. Stress distribution in all directions ($v=5026\text{m/min}$).

3.1.1. The influent of cutting speed for the stress field. As is shown in figure 4, with the cutting speed increasing the magnitudes of crushing stress in all directions fluctuate near -950Mpa first, and then increase at the speed of 3000m/min. The magnitude of Stress-XX is slightly bigger than Stress-YY.

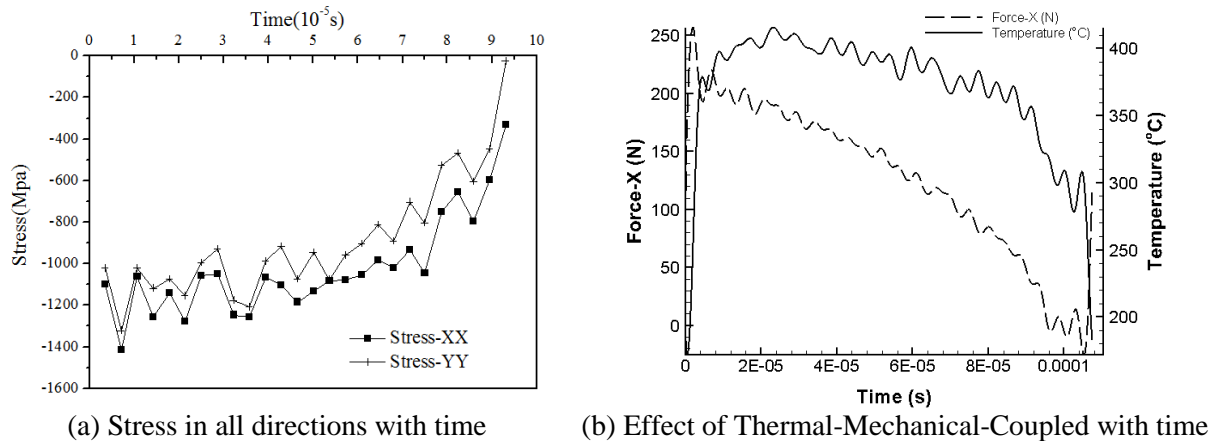


Figure 3. Dynamic distribution of the physical parameters.

Figure 5 illustrates the change of residual stress in machined layer with the cutting speed. The layer 0.03~0.2mm beneath the surface introduces the residual crushing stress and the magnitude is increase with the cutting speed. The residual pulling stress 0.03mm beneath the surface has been found and the magnitude also increases with the cutting speed. This may because the temperature increases with the cutting speed. The residual pulling stress caused by thermal stress occupies a leading position. But the cutting forces reduce with cutting speed within certain limits. The plastic deformation, therefore, reduces. So the magnitude of the residual pulling stress 0.03mm beneath the surface increases with the cutting speed.

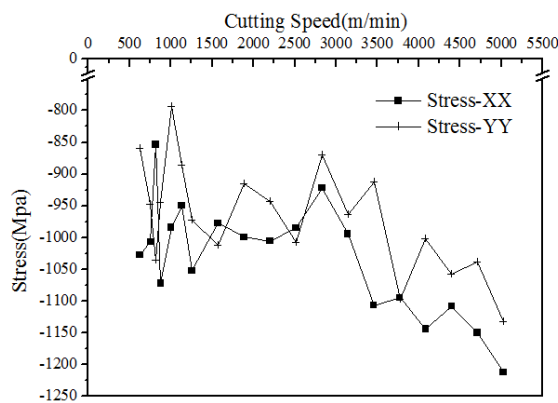


Figure 4. Stress with cutting speed.

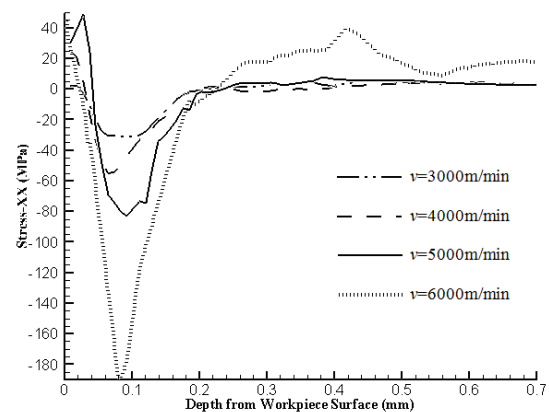


Figure 5. Residual stress with depth from surface.

3.1.2. Experimental verification. Comparing the cutting force of Numerical Simulation with cutting tests' results, the modeling of the system is reasonable. Figure 6 is the cutting force experiment at a speed of 1500m/min. Figure 7 is the curve of the vibratory cutting force getting through the experiments and finite element simulation of cutting force.

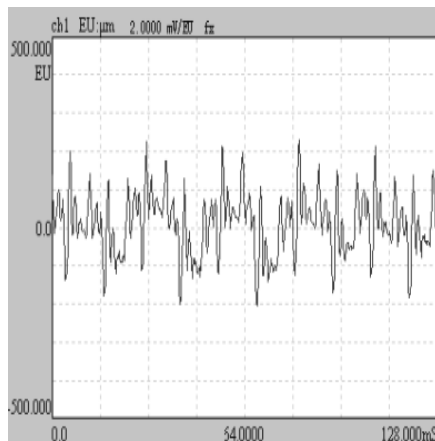


Figure 6. Cutting force of experiment.

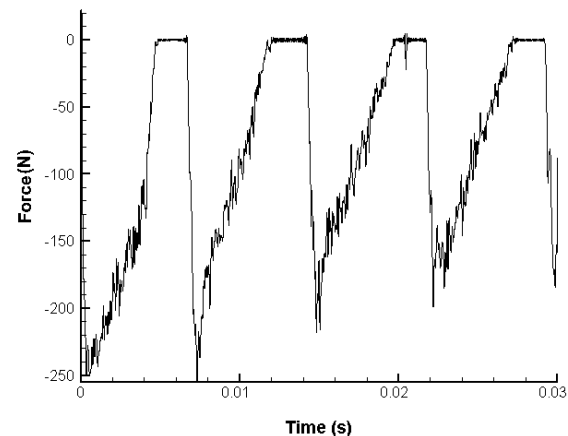


Figure 7. Cutting force of FEM.

During milling process, the continuous cutting of cutting tool is the repeat of this cutting period. The cutting force curve form the test in figure 7 is a periodic change of the milling tools' in and out. And because of the vibration of the tool and machine tool, the cutting force is existent instead zero in theoretical. Simulation of cutting process is a continuous cutting process. Comparing with the experiment, we can get the conclude that the trends change over time in cutting force curve by experiment and simulation are in good agreement.

4. Conclusions

This work builds three-dimensional numerical simulation model by means of FEA software to analysis the stress field of the machined layer. Conclusions are as following:

- (1) The stress field is very complex during the initial phase of the cutting process, which shows the phenomenon of interlacing pulling stress and crushing stress. With the cutting process development, the stress field converts to the stress state that crushing stress occupies a leading position;
- (2) The magnitudes of crushing stress in all directions reduce with milling processes as the effect of Thermal-Mechanical-Coupled weakens;
- (3) With the cutting speed increasing the magnitudes of crushing stress in all directions fluctuate near -950Mpa first, and then increase at the speed of 3000m/min;
- (4) The residual pulling stress 0.03mm~0.2mm beneath the surface has been found and the magnitude increases with the cutting speed.

5. References

- [1] Sun Y Z, Liu H T and Lu Z S 2011 J. Mech. Eng. **47**(1) 187-93.
- [2] Yang K, Liang Y C, Zheng K N, Bai Q S and Chen W Q 2011 Int. J. Adv. Manuf. Tech. **52** 905-12.
- [3] Yang G, Saldana C, Compton W D, et al. 2011 *Acta Mater.* **59** 4538-47.
- [4] Yang G, Efe M, Moscoso W, et al. 2012 *Scrip. Mater.* **66** 235-8.
- [5] Che-Haron C H and Jawaid A. 2005 J. Mater. Proc. Tech. **166**(2) 188-92.
- [6] Rotella G, Dillon O W, Umbrello D, et al. 2013 J. Manuf. Proc. **15** 87-95.
- [7] Yang G, Saldana C, Mann J B, et al. 2011 Adv. Mater. Res. **223** 325-31.
- [8] Zhang H J, Wen W D and Cui H T 2011 Trans. Nanjing Univ. Aeronaut. Astronaut. **28**(1) 81-6.
- [9] Zain A M, Haron H and Sharif S 2010 Exp. Syst. Appl. **37** 4650-9.
- [10] Danisa I, Wojtowicz N, Monies F et al. 2013 *Proc. Eng.* **63** 36-44.
- [11] Chan C Y, Lee W B and Wang H 2013 Int. J. Mach. Tool. Manuf. **73** 62-70.
- [12] Fu X L, Ai X, Liu Z Q and Wan Y 2007 China Mech. Eng. **18**(2) 220.
- [13] Johnson G R and Cook W H, 1985 Eng. Fract. Mech. **21** 31-48.
- [14] Fu X L, Ai X, Wan Y and Zhang S 2007 Trans. Nanjing Univ. Aeronaut. Astronaut. **24**(2) 139-44.

Acknowledgments

The research was supported by National Natural Science Foundation of China (51675262) and also supported by the Advance research field fund project of China (6140210020116H K02001) and the Project of National Key Research and Development Plan of China “New energy-saving environmental protection agricultural engine development” (2016YFD0700800).